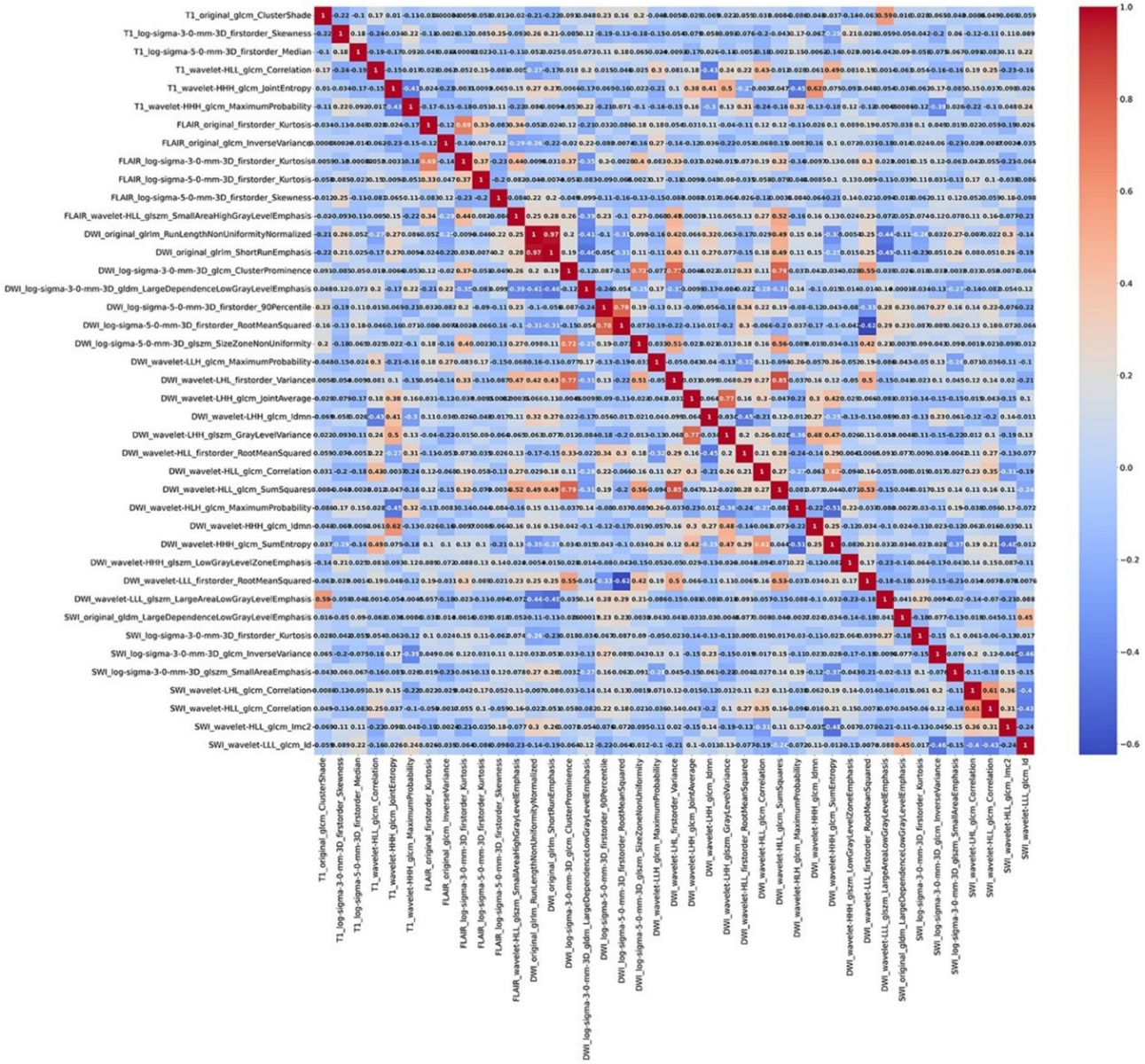

Figure S1 The heat map of feature correlation coefficient after feature selection.

https://dx.doi.org/10.21037/tcr-24-1147

Table S1 The scan parameters of each MRI sequence

MRI sequence	Scan parameters
FLAIR	TR =8,000 ms, TE =150 ms, TI =2,200 ms, NEX =1, flip angle =150°, matrix =256×256
DWI	TR =4,156 ms, TE =114 ms, number of signal averages =4, flip angle =90°, section thickness =5 mm, matrix =152×121, and FOV =230×184 mm^2, b-values =0 and 1,000
CE-T1WI	TR =2,050 ms, TE =24 ms, NEX =1, matrix =256×256
CE-SWI	TE =19.7 ms, TR =27 ms, flip angle =15°, bandwidth (BW) =140 Hz/px, acquisition matrix = 320×240×52, slice thickness 3 mm, FOV 230 mm and voxel size =0.72 mm × 0.72 mm × 2.5 mm

MRI, magnetic resonance imaging; FLAIR, fluid-attenuated inversion recovery; DWI, diffusion weighted imaging; CE-T1WI, contrast-enhanced T1 weighted imaging; CE-SWI, contrast-enhanced susceptibility weighted imaging; TR, time of repetition; TE, time of echo; TI, time of inversion; NEX, number of excitations; FOV, field of view.

Table S2 The number distribution of radiomics features extracted in different image types

Image Type	Shape feature	First-order feature	High-order texture feature	Total
Original images	14	18	68	100
LoG-sigma-transformed images	0	36	136	172
Wavelet-transformed images	0	144	544	688
Total	14	198	748	960

Table S3 Hyperparameter values of each model used in the prediction task

Model	Hyperparameter values
LR	penalty = 'l1', solver = 'liblinear', max_iter =1,000
RF	n_estimators =46
SVM	kernel = 'rbf', C=8, gamma =0.0005, probability = true
XGBoost	n_estimators =25, objective = 'binary: hinge', use_label_encoder = false

LR, logistic regression; RF, random forest; SVM, support vector machine; XGBoost, extreme gradient boosting.

https://dx.doi.org/10.21037/tcr-24-1147

Table S4 The statistic test of selected radiomics features from four MRI sequences in the training set and validation set

Radiomics features	P value	
	Training set	Testing set
FLAIR-original_firstorder_Kurtosis	0.01	0.04
FLAIR-original_glcm_InverseVariance	0.02	0.05
FLAIR-log-sigma-3-0-mm-3D_firstorder_ Kurtosis	0.02	0.02
FLAIR-log-sigma-5-0-mm-3D_firstorder-Kurtosis	0.02	0.02
FLAIR-log-sigma-5-0-mm-3D_firstorder-Skewness	0.01	0.13
FLAIR-wavelet-HLL_glszm_SmallAreaHighGrayLevelEmphasis	0.01	0.14
DWI-original_glrlm_RunLenghthNonUniformityNormalized	0.000	0.02
DWI-original_glrlm_ShortRunEmphasis	0.000	0.04
DWI-log-sigma-3-0-mm-3D_glcm_ClusterProminence	0.03	0.11
DWI-log-sigma-3-0-mm-3D_gldm_LargeDependenceLowGrayLevelEmphasis	0.007	0.02
DWI-log-sigma-5-0-mm-3D_firstorder_90Percentile	0.02	0.07
DWI-log-sigma-5-0-mm-3D_firstorder_RootMeanSquared	0.004	0.02
DWI-log-sigma-5-0-mm-3D_glszm_SizeZoneNonUniformity	0.04	0.10
DWI-wavelet-LLH_glcm_ MaximumProbability	0.02	0.03
DWI-wavelet-LHL_firstorder_Variance	0.02	0.05
DWI-wavelet-LHH_glcm_Joint Average	0.03	0. 03
DWI-wavelet-LHH_glcm_Idmn	0.02	0.003
DWI-wavelet-LHH_glszm_GrayLevelVariance	0.05	0.045
DWI-wavelet-HLL_firstorder _RootMeanSquared	0.02	0.12
DWI-wavelet-HLL_glcm_Correlation	0.004	0.001
DWI-wavelet-HLL_glcm_SumSquares	0.01	0.02
DWI-wavelet-HLH_glcm_MaximumProbability	0.04	0.02
DWI-wavelet_HHH_glcm_Idmn	0.04	0.008
DWI-wavelet-HHH_glcm_SumEntrophy	0.02	0.04
DWI-wavelet-HHH_glszm_LowGrayLevelZoneEmphasis	0.02	0.03
DWI-wavelet-LLL_firstorder _RootMeanSquared	0.05	0.03
DWI-wavelet-LLL_glszm_LargeAreaLowGrayLevelEmphasis	0.02	0.04
CE-T1WI-original_glcm_ClusterShade	0.04	0.058
CE-T1WI-log-sigma-3-0-mm-3D_firstorder_Skewness	0.03	0.043
CE-T1WI-log-sigma-5-0-mm-3D_firstorder_Median	0.02	0.14
CE-T1WI-wavelet-HLL_glcm_Correlation	0.008	0.03
CE-T1WI-wavelet-HHH_glcm_JointEntrophy	0.04	0.07
CE-T1WI-wavelet-HHH_glcm_MaximumProbability	0.02	0.02
CE-SWI-original-gldm_LargeDependenceLowGrayLevelEmphasis	0.02	0.007
CE-SWI-log-sigma-3-0-mm-3D_firstorder_Kurtosis	0.01	0.03
CE-SWI-log-sigma-3-0-mm-3D_glcm_ InverseVariance	0.02	0.07
CE-SWI-log-sigma-3-0-mm-3D_glszm_SmallAreaEmphasis	0.02	0.005
CE-SWI-wavelet-LHL_glcm_Correlation	0.03	0.004
CE-SWI-wavelet-HLL_glcm_Correlation	0.03	0.003
CE-SWI-wavelet-HLL_glcm_Imc2	0.04	0.000
CE-SWI-wavelet-LLL_glcm_Id	0.03	0.000

https://dx.doi.org/10.21037/tcr-24-1147